Ring structure of selected two-dimensional procrystalline lattices

David Ormrod Morley [1], Andrew L. Goodwin [2], and Mark Wilson [1,*]

[1]*Department of Chemistry, Physical and Theoretical Chemistry Laboratory, University of Oxford,
South Parks Road, Oxford OX1 3QZ, United Kingdom*

[2]*Department of Chemistry, Inorganic Chemistry Laboratory, University of Oxford, South Parks Road, Oxford OX1 3QR, United Kingdom*

Recent work has introduced the term "procrystalline" to define systems which lack translational symmetry but have an underlying high-symmetry lattice. The properties of five such two-dimensional (2D) lattices are considered in terms of the topologies of rings which may be formed from three-coordinate sites only. Parent lattices with full coordination numbers of four, five, and six are considered, with configurations generated using a Monte Carlo algorithm. The different lattices are shown to generate configurations with varied ring distributions. The different constraints imposed by the underlying lattices are discussed. Ring size distributions are obtained analytically for two of the simpler lattices considered (the square and trihexagonal nets). In all cases, the ring size distributions are compared to those obtained via a maximum entropy method. The configurations are analyzed with respect to the near-universal Lemaître curve (which connects the fraction of six-membered rings with the width of the ring size distribution) and three lattices are highlighted as rare examples of systems which generate configurations which do not map onto this curve. The assortativities are considered, which contain information on the degree of ordering of different sized rings within a given distribution. All of the systems studied show systematically greater assortativities when compared to those generated using a standard bond-switching method. Comparison is also made to two series of crystalline motifs which shown distinctive behavior in terms of both the ring size distributions and the assortativities. Procrystalline lattices are therefore shown to have fundamentally different behavior to traditional disordered and crystalline systems, indicative of the partial ordering of the underlying lattices.

I. INTRODUCTION

Disordered two-dimensional networks appear common in nature (covering, for example, foams [1,2], biological cells [3,4], and rock formations [5,6]). Significant progress has been made in manipulating materials at low dimensionality such as nanoparticular colloids [7,8] and ultrathin materials (including, for example, amorphous graphene [9,10], and bilayers of silica [11,12], aluminosilicates [13], and germania [14]). The ability to effectively manipulate these materials and hence control key properties such as the pore sizes and their spatial distribution [15] (which could prove useful for gas separation and water filtration) requires a detailed understanding of the possible structures which may form in two dimensions and the length scales on which order becomes suppressed.

The expansion in experimental imaging capabilities, modeling methodologies, and computer power are starting to challenge the idea that all these systems behave as continuous random networks (CRNs). Recent work has defined a range of systems as "procrystalline" in that they lack translational symmetry and yet have structures which can be rationalized in terms of an underlying high symmetry lattice [16]. For example, Fig. 1 illustrates a typical procrystal based on the square lattice. Procrystals consist of a regular array of lattice points in real space but contain defects in dual space. Each node

in real space has the same coordination number but different orientations of the connections. Therefore, while procrystals appear crystalline in their atomic radial distribution function (RDFs) and structure factors, the difference between the atom coordination number and the natural coordination of the underlying lattice leads to disorder in the ring structure. As such, they can be considered to sit somewhere in between crystals and CRNs, which as we will show is detectable in their network properties. Experimentally they occur in self-assembled molecular monolayers [17], classical bond valence solids [18], mixed-anion perovskites [19], and order-disorder ferroelectrics [20].

Disordered networks of percolating rings may be generated starting from a high symmetry lattice. In the context of atomic networks, a ring is any closed path of sequentially linked atoms, but the term is used here in reference only to the primitive rings, i.e., those which cannot be subdivided into two smaller rings [21]. If the resulting networks contain only three-coordinate sites, then the mean ring size will be six, originating in Euler's formula for connected planar graphs:

$$V + F - E = \chi, \tag{1}$$

where V, F, and E are the numbers of vertices, faces, and edges respectively and χ is a topology-specific integer termed the Euler characteristic. If the system is 2D and periodic with three-coordinate sites, $\chi = 0$ and $E = 3V/2$ so that the result $3V/F = 6$ readily follows [22]. For aperiodic systems, $\chi = 1$ and the mean ring size of six is quickly approached as the total
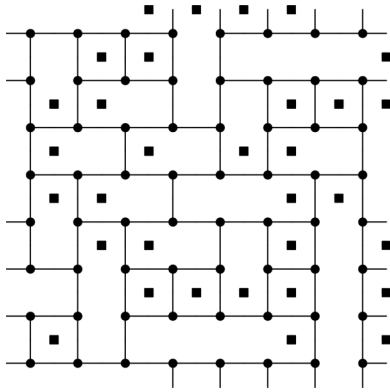
*mark.wilson@chem.ox.ac.uk

FIG. 1. Example of a procrystal based on the square lattice. The regular array of nodes (black circles) each have exactly three links forming the procrystalline network. The nodes of the dual lattice (black squares) are also displayed and can be viewed as square lattice with defects.

number of rings increases. In this paper, we will highlight how disordered and diverse networks of percolating rings may be generated from different underlying high-symmetry lattices. Each lattice imposes different constraints on the ring structure. In simpler cases, the structures adopted by relatively small systems may be understood purely analytically. For more complex and/or larger systems, a Monte Carlo method can be employed to generate configurations.

Our paper is arranged as follows. We begin by detailing the series of two-dimensional procrystalline lattices at the heart of our study, including the methods we use to generate them and to characterize their corresponding ring statistics. In our results section, we report these ring statistics, calculated using both analytical and numerical methods, taking into account also the effect of system size. Our key results concern the second moments of the ring distributions and the corresponding assortativities, which we show differ fundamentally for procrystals from those for crystals, on the one hand, and CRNs, on the other. We conclude with a brief discussion of the implications of our results in a more general context.

II. METHODS

Figures 2(a)–2(e) shows the five tilings considered here, which can be divided in terms of the coordination number of the original tilings (here four-, five-, and six-coordinate) and occur across a variety of experimental and theoretical studies. The four-coordinate tilings considered are the square [23–25] and trihexagonal (also known as kagome) [26–28] nets, the five-coordinate tilings are the elongated-triangular [29] and snub-square nets [30–33], and the six-coordinate tiling is a triangular net. Each n-coordinate tiling can generate connected procrystals with m-coordinate nodes in the range $m = 3 \rightarrow (n - 1)$. We will therefore adopt the nomenclature n, m lattice when referring to specific procrystals, in order to highlight their coordination properties and underlying lattice; e.g., the configuration in Fig. 1 is a 4,3-square procrystalline lattice. Interestingly, the allowable rings and ring statistics seem to depend both on the underlying lattice and the coordination number. In the present work, we focus purely on the
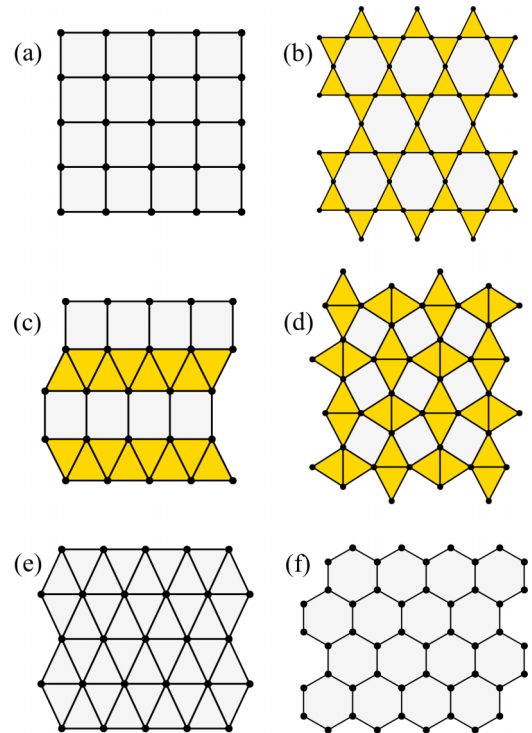

FIG. 2. The five crystalline lattices considered here: (a) square, (b) trihexagonal, (c) elongated-triangular, (d) snub -square, and (e) triangular tiling. Panel (f) shows the hexagonal net, which is the basis for the bond-switching algorithm described in the text.

three-coordinate configurations, as these are most prevalent in nature, and so making contact with previous work [22,34,35].

In the 4,3-square procrystalline lattice, in which atoms located on a regular square lattice possess only three bonds, the configurational space would be expected to grow exponentially quickly: naively as 4^N if each atom is a T shape which can take anyone of four orientations. However, the space is actually significantly contracted under the condition the atoms all achieve full coordination (i.e., there are no dangling bonds). A consequence of this statement is that it also enforces periodicity. This is in analogy with classic problems of arranging dimers on a lattice [36,37]. The number of configurations still grows very rapidly, but the problem becomes computationally tractable for a greater range of lattice sizes.

Mapping the configurational space can be achieved by two approaches. The first is by using exact tiling to obtain all the possible configurations for a given lattice size. The second is Monte Carlo sampling, discussed below, which allows the distribution of lattices of any size to be sampled. The former is feasible only for relatively small systems but may provide useful insight into the topologies of larger systems. In addition it is interesting to compare these procrystalline lattices to more "conventional" three-coordinate amorphous materials, which are still required to have a fixed mean ring size but have fewer geometric constraints.

A. Monte Carlo

A zero-temperature Monte Carlo optimization algorithm was developed to sample the configurational space for the
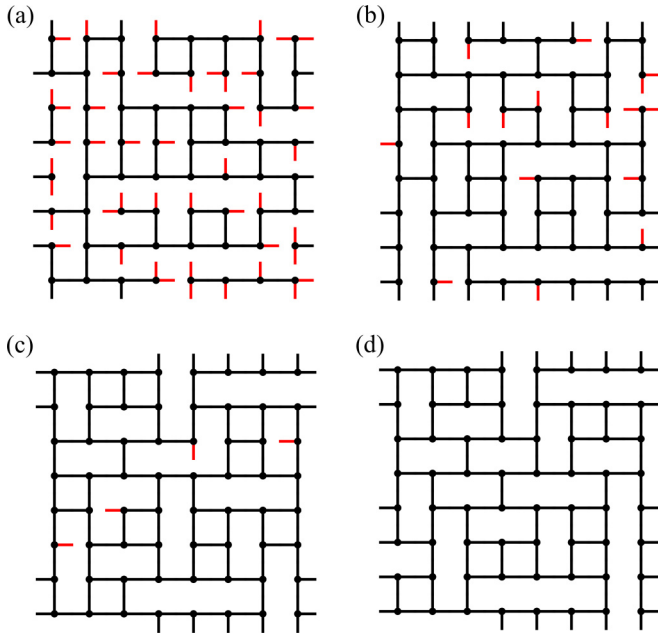
(a)

(b)

(c)

(d)

FIG. 3. Panels (a)–(d) show snapshots from the generation of a configuration of a 4,3-square lattice via a Monte Carlo method. As the algorithm progresses, dangling bonds (highlighted in red) are removed until full coordination is achieved.

different procrystalline lattices. The algorithm proceeds as follows:

(1) For the starting structure, take a periodic lattice from Fig. 2 and randomly assign each node three bonds from the possible orientations defined by the underlying lattice. This will introduce a number of dangling bonds into the configuration.

(2) Select a node at random and change the three bonds.

(3) If the number of dangling bonds is less than or equal to the number in the previous configuration, update the configuration; otherwise, revert to the previous structure.

(4) Repeat steps 2 and 3 until all dangling bonds have been removed and all node coordinations are satisfied. The final lattice is then in the procrystalline state.

This process is demonstrated for an 8×8 square lattice in Fig. 3. As removing the dangling bonds often requires a correlated motion, it becomes increasingly difficult to remove defects as they reduce in number. Furthermore the structure obtained with a small number of dangling bonds can be quite different to the final procrystalline network as a consequence of the required reorganization.

This method can be thought of as a simplified version of a site adsorption model, where molecules adsorb to specific sites on an underlying lattice and interact with varying directional potentials [38–40]. The difference is that here the potential model is binary and the aim of the method is to generate a fully coordinate, defect-free "ground state" procrystalline lattice. One could in principle introduce a Metropolis-type criterion into step 3 [41], where moves are accepted according to max[1, exp $(-\Delta U/k_B T)$], with ΔU as the change in number of dangling bonds and T as a temperature parameter. This modification would allow a proportion of "uphill" moves, where the number of dangling bonds in-

creases, in contrast to the $T = 0$ case when only "downhill" moves, which maintain or reduce the number of dangling bonds, are accepted. However, we found the zero-temperature version to converge very well, as there is sufficient flexibility through moves which merely conserve the number of dangling bonds for a global minimum to be reached. In addition, the temperature parameter was not found to appreciably affect the overall properties of the resulting realisations.

In this work, we used this Monte Carlo method to generate configurations for each of the five underlying lattice types, with number of nodes in the lattice scaled to explore system size effects. For each set of parameters, some 10^5 periodic procrystalline lattices were generated.

B. Bond switching

As a complement to the work on procrystalline lattices, we will compare results with amorphous three-coordinate lattices. Computational configurations of two-dimensional CRNs of this type can be generated using a bond-switching algorithm. This algorithm is described in detail in Ref. [22] and references therein, but can be summarized as follows. The algorithm starts with a pristine hexagonal lattice, as in Fig. 2(f). Connections between neighboring atoms are then switched in such a way to introduce defects, while preserving the overall atomic coordination number. As successive defects overlap, the initial memory of the crystalline lattice is lost and an amorphous structure results.

Previously, this algorithm has been employed in a manner analogous to simulated annealing, where the random amorphous structure is then cooled to generate physically motivated realizations of network-forming materials, which have significant enthalpic constraints [22,42,43]. To compare to the procrystalline lattices, however, we are only interested in the highest entropy solutions and so effectively run the bond switching continually at infinite temperature, until the required sampling is reached. This generates configurations which are highly unphysical from a materials perspective but provide a useful comparison point as a high entropy lattice which is amorphous both in real and dual space.

An example of a highly disordered CRN produced from bond switching is given in Fig. 4(f). The primary difference when compared to the procrystalline configurations is that the atomic positions are not constrained to a lattice and are free to migrate. Atoms are therefore also able to form bonding connections to other species outside the original nearest neighbors defined by the starting hexagonal lattice. For a lattice of a given size, 10^4 configurations were sampled, starting from 100 different starting seeds.

C. Ring statistics

Given it is the rings which are the source of disorder in procrystalline lattices, we must quantify the level of disorder through the ring structure. As previously mentioned, the mean ring size is insufficient, as for three-coordinate atoms it is constrained to six by Euler's formula. The main measure of disorder is therefore the ring size distribution itself, p_k, and its associated second moment, $\mu_2 = \langle k^2 \rangle - \langle k \rangle^2$ [44].
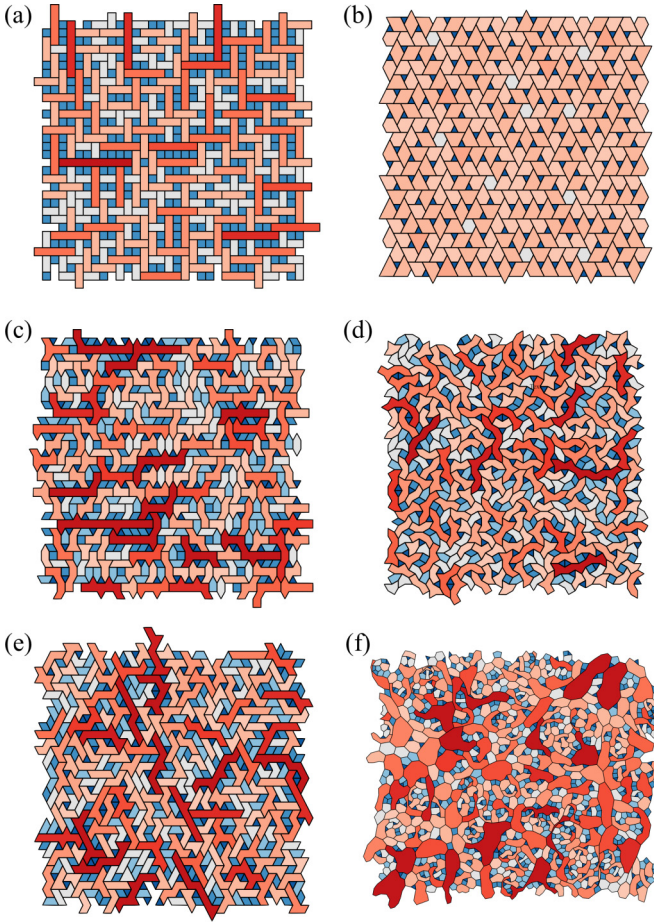
FIG. 4. Example configurations generated using the Monte Carlo procedure as described in the text. Six-membered rings are shown in gray, while rings with size $k < 6$ are shown as light to dark blue for decreasing k, and rings of size $k > 6$ are shown as light to dark red for increasing k. The configurations are shown in the same order as for Fig. 2.

As a reference, we can compare to the maximum entropy ring distribution. This approach was used by Lemaître *et al.* as part of the study of generic CRNs [45]. The entropy of a given ring distribution is given by

$$S = -\sum_k p_k \ln p_k, \quad (2)$$

to which the following constraints may then be applied:

$$\sum_k p_k = 1, \quad (3)$$

$$\sum_k k p_k = 6, \quad (4)$$

$$\sum_k p_k / k = \text{constant}. \quad (5)$$

The first constraint simply arises from the normalization condition, the second reflects the constrained mean ring size, while the third was argued on the basis of empirical observations of ring areas. The maximum entropy solution, which we denote P_k, can be found subject to these constraints by using

TABLE I. Theoretical values of the proportion of hexagons and variance for the maximum entropy ring size distributions in different procrystalline lattices.

Procrystal	P_6	μ_2
4,3-square	0.250	8.0
6,3-triangular	0.105	12.0
4,3-trihexagonal	0.021	4.75

Lagrange's method to find

$$P_k = \frac{e^{-\lambda_1 k - \lambda_2 / k}}{\sum_k e^{-\lambda_1 k - \lambda_2 / k}}, \quad (6)$$

which can be solved numerically by substitution into Eq. (4). This forms the basis of Lemaître's law, which will be discussed in Sec. III and has been shown to hold for a wide range of CRNs [22,46,47].

For the procrystalline lattices discussed in this work, a similar approach may be taken, except the process is somewhat simpler because the constraint (5) does not apply. Removing this constraint, we find a modification of Eq. (6) where $\lambda_2 = 0$:

$$P_k = \frac{e^{-\lambda k}}{\sum_k e^{-\lambda k}}. \quad (7)$$

An important additional constraint arises implicitly through the k range in the summation. In the most general case, the set of k values is $\{3, 4, 5 \ldots\}$, as the smallest ring is the triangle. Under these conditions, we find that the maximum entropy ring distribution, which we denote P_k, is given by

$$P_k = \left(\tfrac{1}{4}\right)\left(\tfrac{3}{4}\right)^{k-3}, \quad k \in \{3, 4, 5 \ldots\}. \quad (8)$$

However, this can easily be modified to suit the underlying lattice conditions. For example, in the 4,3-square lattice, only even rings are permissible such that the k values are $\{4, 6, 8 \ldots\}$, where the smallest ring is the now the square. Under these conditions, we find the maximum entropy distribution is

$$P_k = \left(\tfrac{1}{2}\right)^{k/2-1}, \quad k \in \{4, 6, 8 \ldots\}. \quad (9)$$

The maximum entropy distribution solutions for three lattice types are summarized in Table I.

D. Assortativity

While the ring distribution is highly informative, it is a global measure and gives no insight into the ring adjacencies. Therefore, an additional metric can be used to gain information on nearest-neighbor correlations. One could use empirical measures such as the Aboav-Weaire law [48], but in this work we will use the assortativity, a well-defined metric from network theory, which measures the tendency for large rings to be adjacent to small rings. To calculate the assortativity requires construction of the joint degree distribution, with each element e_{jk} giving the probability of a ring of size j being adjacent to a ring of size k. The assortativity is then quantified
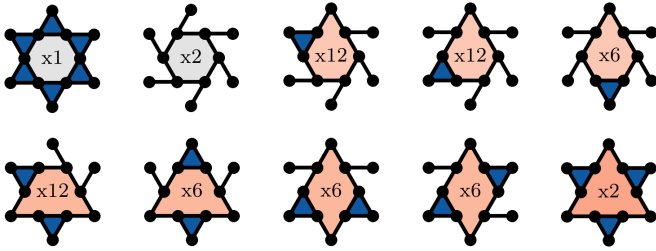
FIG. 5. The ten possible ring configurations obtained for a small unit ($V = 12$) of the trihexagonal lattice. The value at the center of each panel is the configuration degeneracy.

through the Pearson correlation coefficient,

$$r = \frac{\langle k \rangle^2 \sum_{jk} jk e_{jk} - \langle k^2 \rangle^2}{\langle k \rangle \langle k^3 \rangle - \langle k^2 \rangle^2}, \tag{10}$$

where $-1 \leqslant r \leqslant 1$ [49]. A negative value of r indicates an increased preference for large rings to be adjacent to small rings, when compared to a purely random arrangement. Conversely, a positive value of r indicates an increased likelihood for similar sized rings to be grouped.

III. RESULTS

The networks based on underlying four-coordinate lattices may be considered in an analytic fashion, as in the first subsection below. However, the commensurate analysis for the five- and six-coordinate lattices is much more complex and so must be considered using the Monte Carlo procedure, as described in the second subsection below.

A. Exact tilings

The 4,3-square and 4,3-trihexagonal lattices are both four-coordinate and so the underlying constraints associated with forming three-coordinate networks can be considered analytically. Taking first the 4,3-square lattice (which is perhaps the simplest lattice considered here to rationalize). The lack of "cross" bonds (acting between opposite corners of a square) in the lattice means that only even-membered rings are possible. Rings must be linear as any "L" shapes require stabilization of a two-coordinate site.

For the 4,3-trihexagonal lattice, the constraints imposed are perhaps more difficult to rationalize, with only ring sizes in the set $k = \{3, 6, 7, 8, 9\}$ allowed while maintaining three-coordination. A lattice of V vertices will have $2V$ edges and V faces, $\frac{2V}{3}$ of which are triangles [from Euler's formula (1)]. Generating the procrystal requires removal of $\frac{V}{2}$ edges, leaving $\frac{V}{2}$ faces. Each edge removed must necessarily remove one triangle only, so that the final number of triangles is $\frac{V}{6}$ and hence $p_3 = \frac{1}{3}$.

In addition to the highly constrained set of allowed ring sizes, the relative frequencies of these rings are not equal. In order to rationalize this, we must consider the number of ways of achieving each ring size. Figure 5 takes a small unit of the kagome lattice, with 12 vertices, and shows the possible ways of producing each ring, with the number of symmetry related species indicated in the center of each cell. This analysis

predicts a ratio of $1 : 15 : 15 : 1$ for $p_6 \rightarrow p_9$. This now fully constrains the problem, and we find

$$P_3 = \tfrac{1}{3}, \quad P_6 = \tfrac{1}{48}, \quad P_7 = \tfrac{5}{16}, \quad P_8 = \tfrac{5}{16}, \quad P_9 = \tfrac{1}{48}. \tag{11}$$

Figure 5 also highlights further effects of the high symmetry lattice. First, $k = 9$ is the largest ring which can be supported as any larger ring would require the stabilization of two-coordinate sites. Second, a k ring must be nearest neighbors with k-6,3-membered rings, for $k \geqslant 6$.

In addition to determining the ring statistics, the assortativity for the maximum entropy solution of the 4,3-trihexagonal lattice can be investigated. The joint degree distribution in this case is given by

$$\mathbf{e} = \frac{1}{96} \begin{bmatrix} 0 & 0 & 5 & 10 & 1 \\ 0 & 0 & 1 & 1 & 0 \\ 5 & 1 & 14 & 14 & 1 \\ 10 & 1 & 14 & 14 & 1 \\ 1 & 0 & 1 & 1 & 0 \end{bmatrix} \begin{matrix} 3 \\ 6 \\ 7 \\ 8 \\ 9 \end{matrix}, \tag{12}$$

which can be rationalized as follows. The sum of each row is given by $\sum_k e_{jk} = k p_k / 6$ such that the entire matrix is normalized. In addition, as each neighboring ring adjacency is reciprocated, $e_{jk} = e_{kj}$. The value of the specific elements can be deduced by careful inspection of Fig. 5. For example, zeros appear where the lattice constraints prevent the neighboring of two ring sizes. Using this matrix in Eq. (10) gives a value of $r = -101/367 \approx -0.275$, i.e., the 4,3-trihexagonal lattice is disassortative. We see this is consistent and intuitive with the previous observation that larger rings are surrounded by an increasing number of three-rings.

B. Monte Carlo

Figure 4 shows example configurations generated using the MC procedure described above. The different ring sizes are highlighted by different colors as indicated in the figure caption. The constraints on the ring sizes imposed by the underlying lattices are evident in a number of cases. For example, the linear rings are evident in the configuration obtained for the 4,3-square lattice [Fig. 4(a)] but are also clear in that obtained for the 5,3-elongated-triangular tiling [Fig. 4(c)]. In addition, the limited ring size set permissible in the 4,3-trihexagonal lattice is also clear. Figure 4(f) shows a typical amorphous configuration obtained from bond switching. Note that the use of an effective infinite temperature to generate these configurations results in relatively unphysical (unconstrained) configurations which feature, for example, highly nonconvex structures. In general, the effect of the underlying lattices in generating novel ring structures is clear.

Figure 6 shows the ring distributions generated for the three-coordinate networks starting from the five lattices shown in Fig. 2 as well as from bond switching. These distributions act to highlight how the different tilings impose additional (different) constraints. As discussed above, for the 4,3-square lattice only even-membered rings are allowed (three-dimensional distributions with this constraint having been generated previously [50]). The 4,3-square lattice cell
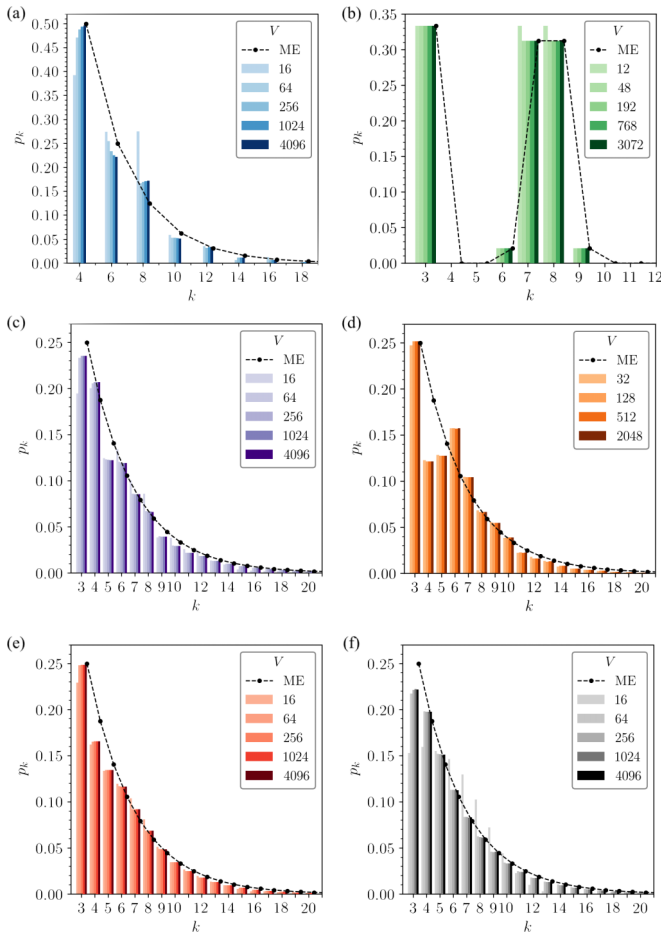
FIG. 6. Ring size distributions for the five crystalline lattices considered here. Key: (a) 4,3-square, (b) 4,3-trihexagonal, (c) 5,3-elongated-triangular tiling, (d) 5,3-snub-square, and (e) 6,3-triangular. Panel (f) shows the results of configurations obtained from bond switching. In all panels, the points and dashed lines show the respective maximum entropy (ME) solutions. Each panel also highlights potential system size effects by showing the ring size distributions for different numbers of nodes, V, as highlighted in the legends.

for $V = 16$ is small enough to explicitly show the possible configurations (see Fig. S1 in the Supplemental Material [51]). For the 4,3-trihexagonal lattice, only rings of size $k = \{3, 6, 7, 8, 9\}$ are allowed. Distributions of this general form have been observed previously, for example, for a model using a core-softened potential and long-range repulsions [52], and for models of BN nanotubes encased in amorphous material [53]. The figures also show the ME solutions. The constraints discussed above for the square and 4,3-trihexagonal lattices are clear. However, it is also clear that the snub and elongated triangular lattices show the more subtle effects of the underlying constraints. There are some similarities between the different ring distributions. For example, the 5,3-snub-square and 6,3-triangular lattices [Figs. 6(d) and 6(e)] both show fewer four- and five-membered rings, and more six- and seven-membered rings, when compared to the ME solutions. In general, the distributions become more like the ME solutions on moving from an underlying four- to five-
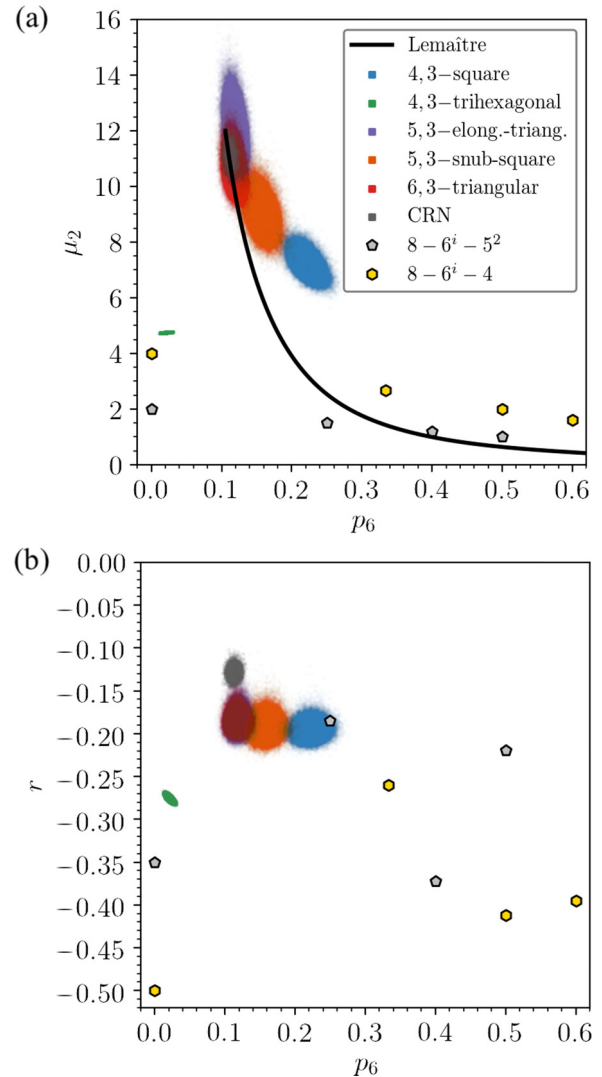

FIG. 7. The values of the (a) second moment, μ_2, and (b) assortativity, r, as a function of the fraction of six-membered rings, p_6, for configurations generated on the five lattices considered here as well as those generated by bond switching. These are colored as indicated in the captions, but if viewing in grayscale, note that the each lattice can be identified by comparing to the p_6 values given in Fig. 6.

to six-coordinate lattice, reflecting the decrease in constraints along that pathway. Figure 6(f) shows the ring statistics from the bond-switching algorithm (and hence corresponding to a high-temperature CRN). It is clear that the configurations generated with the procrystalline constraints are fundamentally different purely in terms of the underlying ring statistics.

Figures 7(a) and 7(b) show the values of μ_2 and r as a function of p_6 for the three-coordinate configurations generated from the five lattices. For completeness, details of the observable system size effects can also be found in the Supplementary Material [51]. These are presented alongside data from bond switching, representing generic CRNs, and with two series of crystalline motifs of the form 8-6^i-5^2 and 8-6^i-4 for $0 \leqslant i \leqslant 3$ (the nomenclature indicating the number of each ring size in the unit cell) [54]. For four

procrystalline lattices (excepting the 4,3-trihexagonal case), the width of the ring size distribution, as characterized by the second moment, increases as p_6 decreases. The four cases lie toward the high-μ_2 limit of the Lemaître curve which lies at $p_6 = 0.105$. The systems lie of the upper end of this curve as the formation of arbitrarily large rings is not precluded on enthaplic grounds. The configurations generated on the 4,3-trihexagonal lattice are unique here in lying at both a low p_6 and a relatively low μ_2, although much more in keeping with systems constrained so as to preclude the formation of large rings (for example, the two-dimensional crystal constructed purely from four- and eight-membered rings). The 4,3-square lattice configurations show μ_2 values systematically higher than those predicted from the Lemaître curve. For the five-coordinate lattices, the 5,3-snub-square lattice lies at μ_2 values significantly higher than those associated with the Lemaître curve (although less removed than those associated with the square lattice), while the 5,3-elongated-triangular lattice lies at high μ_2, again above the Lemaître curve. The second moments generated from the 6,3-triangular lattice lie near the low-p_6 ME limit of $p_6 \approx 0.105$, occupied by the CRNs.

The deviation of the second moments from the Lemaître curve is therefore correlated with the strength of the constraints imposed by the underlying crystalline lattice (which decrease from four- to five- to six-coordinate). To reiterate, while crystalline lattices are free to locate around the Lemaître curve (their formation usually driven by the energetic landscape) and disorded CRNs constrained to lie upon it, procrystals occupy a region in between these extremes, with the degree of deviation related to the difference in the coordination number of the procrystal and the underlying lattice. In previous work, it was demonstrated how a very wide range of systems (including atomistic networks, nanoparticular packings, geopolitical maps, etc.) generated $\{\mu_2, p_6\}$ data sets which did fit on the Lemaître curve [22]. The configurations generated here are relatively rare examples of systems which do not.

For the assortativities shown in Fig. 7(b), again four of the lattices show similar mean values ($\langle r \rangle \approx -0.19$) corresponding to favoring disassortative configurations. Again, the 4,3-trihexagonal lattice is unique in displaying a highly disassortative $\langle r \rangle \approx -0.275$ as previously rationalized. The bond-switching configurations show a less negative assortativity of $\langle r \rangle \approx -0.13$, whil3 the crystals take up a variety of strongly negative values. The effect of the constraints are, therefore, to impose *greater* short-range ordering on the ring topology. This observation is consistent with the relatively high values of μ_2 [Fig. 7(a)]. The constrained systems promote the formation of large rings (high μ_2) which are then preferentially linked to neighboring small rings (more negative $\langle r \rangle$).

It is clear, therefore, that the procrystalline lattices generate configurations which are fundamentally different from those generated from algorithms based on a continuous random networks and crystalline materials. Previous work has highlighted deviations from generic behavior, for example, in violating the Aboav-Weaire law. Aboav [55] and Boots [56] recognized that a number of regular lattices (of which the crystals highlighted above would be an example) would

violate this law. These regular lattices also do not sit on the Lemaître curve. In addition, the presence of extreme ring sizes and/or edge length distributions have been shown to preclude the linear fit required to satisfy the Aboav-Weaire [57,58]. However, these systems would still sit firmly on the Lemaître curve. The procrystalline configurations described here are the first examples of disordered systems which systematically violate the Lemaître law.

IV. CONCLUSIONS

In this paper, we have considered the ring structures generated from five underlying high symmetry lattices, building configurations which are purely three-coordinate. The effect of the high symmetry lattice is to constrain the ring distributions. The extent of this constraint can be quantified by reference to the maximum entropy solutions and is found to be strongest for the four-coordinate lattices, that is, when only a single connection has to be removed, and weakest for the six-coordinate lattice, for which three connections must be removed. Understandably, therefore, the constraints imposed on the ring size distributions are correlated with the available degrees of freedom when removing connections to form the three-coordinate lattices. The additional effect of the imposed constraints is that several of these networks are examples of systems which do not fit on the Lemaître curve (which links the number of six-membered rings to the width of the ring size distribution). The connectivity of the rings has been explored using the assortativity, with the networks considered showing significantly greater assortativity (ring ordering) than more random networks. The two four-coordinate lattices considered, the 4,3-square and 4,3-trihexagonal, are simple enough to consider analytically for small systems, which provides insight into the configurations favored for larger systems. Furthermore, we have investigated potential system size effects and highlighted how the more constrained systems show ordering which requires larger systems to be fully converged.

If our results are mirrored by equally anomalous ring statistics in three-dimensional procrystalline networks, we might expect a variety of physical properties that depend on correlation to be affected in otherwise unexpected ways. For example, the disordered pore networks of Prussian blue analogs possess topological characteristics that differ meaningfully from those of random or ordered porous media, in turn influencing their transport properties [59]. On a different length scale, photonic procrystals should exhibit photonic band structures different from those of both ordered and amorphous phases [60,61].

[1] M. Durand, J. Käfer, C. Quilliet, S. Cox, S. A. Talebi, and F. Graner, Phys. Rev. Lett. **107**, 168304 (2011).

[2] M. Tong, K. Cole, P. R. Brito-Parada, S. Neethling, and J. J. Cilliers, Langmuir **33**, 3839 (2017).

[3] M. C. Gibson, A. B. Patel, R. Nagpal, and N. Perrimon, Nature (London) **442**, 1038 (2006).

[4] R. Carter, Y. E. Sánchez-Corrales, M. Hartley, V. A. Grieneisen, and A. F. M. Marée, Development **144**, 4386 (2017).

[5] D. Weaire and N. Rivier, Contemp. Phys. **50**, 199 (2009).

[6] L. Goehring and S. W. Morris, Phys. Today **67**(11), 39 (2014).

[7] A. L. Thorneywork, J. L. Abbott, D. G. A. L. Aarts, and R. P. A. Dullens, Phys. Rev. Lett. **118**, 158001 (2017).

[8] L. Isa, I. Buttinoni, M. A. Fernandez-Rodriguez, and S. A. Vasudevan, Europhys. Lett. **119**, 26001 (2017).

[9] J. Kotakoski, A. V. Krasheninnikov, U. Kaiser, and J. C. Meyer, Phys. Rev. Lett. **106**, 105505 (2011).

[10] F. R. Eder, J. Kotakoski, U. Kaiser, and J. C. Meyer, Sci. Rep. **4**, 4060 (2014).

[11] P. Y. Huang, S. Kurasch, A. Srivastava, V. Skakalova, J. Kotakoski, A. V. Krasheninnikov, R. Hovden, Q. Mao, J. C. Meyer, J. H. Smet *et al.*, Nano Lett. **12**, 1081 (2012).

[12] L. Lichtenstein, M. Heyde, and H. J. Freund, Phys. Rev. Lett. **109**, 106101 (2012).

[13] S. Shaikhutdinov and H.-j. Freund, ChemPhysChem **14**, 71 (2013).

[14] A. L. Lewandowski, P. Schlexer, C. Büchner, E. M. Davis, H. Burrall, K. M. Burson, W. D. Schneider, M. Heyde, G. Pacchioni, and H. J. Freund, Phys. Rev. B **97**, 115406 (2018).

[15] C. Büchner and M. Heyde, Prog. Surf. Sci. **92**, 341 (2017).

[16] A. R. Overy, A. B. Cairns, M. J. Cliffe, A. Simonov, M. G. Tucker, and A. L. Goodwin, Nat. Commun. **7**, 10445 (2016).

[17] M. O. Blunt, J. C. Russell, M. C. Giménez-López, J. P. Garrahan, X. Lin, M. Schröder, N. R. Champness, and P. H. Beton, Science **322**, 1077 (2008).

[18] P. W. Anderson, Mater. Res. Bull. **8**, 153 (1973).

[19] P. J. Camp, A. Fuertes, and J. P. Attfield, J. Am. Chem. Soc. **134**, 6762 (2012).

[20] R. Comes, M. Lambert, and A. Guinier, Solid State Commun. **6**, 715 (1968).

[21] X. Yuan and A. N. Cormack, Comput. Mater. Sci. **24**, 343 (2002).

[22] D. Ormrod Morley, A. L. Thorneywork, R. P. A. Dullens, and M. Wilson, Phys. Rev. E **101**, 042309 (2020).

[23] G. Algara-Siller, O. Lehtinen, F. C. Wang, R. R. Nair, U. Kaiser, H. A. Wu, G. A. K, and I. V. Grigorieva, Nature (London) **519**, 443 (2015).

[24] Y. Zhu, F. Wang, and H. Wu, J. Chem. Phys. **147**, 044706 (2017).

[25] S. J. Hibble, A. M. Chippindale, E. J. Bilb, E. Marelli, P. J. F. Harris, and A. C. Hannon, Inorg. Chem. **50**, 104 (2011).

[26] Q.-N. Zheng, L. Wang, Y.-W. Zhong, X.-H. Liu, T. Chen, H.-J. Yan, D. Wang, J.-N. Yao, and L.-J. Wan, Langmuir **30**, 3034 (2014).

[27] L. Postulka, S. M. Winter, A. G. Mihailov, A. Mailman, A. Assoud, C. M. Robertson, B. Wolf, M. Lang, and R. T. Oakley, J. Am. Chem. Soc. **138**, 10738 (2016).

[28] T. Chen, H.-J. Yan, X. Zhang, D. Wang, and L.-J. Wan, Chem. Asian J. **6**, 1811 (2011).

[29] A. D. Griffith and R. S. Hoy, Phys. Rev. E **98**, 042910 (2018).

[30] J. I. Urgel, D. Ecija, W. Auwa, A. C. Papageorgiou, A. P. Seitsonen, S. Vijayaraghavan, S. Joshi, S. Fischer, J. Reichert, and J. V. Barth, J. Phys. Chem. C **118**, 12908 (2014).

[31] N. P. Kryuchkov, S. O. Yurchenko, Y. D. Fomin, E. N. Tsiok, and V. N. Ryzhov, Soft Matter **14**, 2152 (2018).

[32] B.-Q. Song, X.-L. Wang, Y.-T. Zhang, X.-S. Wu, H.-S. Liu, K.-Z. Shao, and Z.-M. Su, Chem. Commun. **51**, 9515 (2015).

[33] W. D. Piñeros, M. Baldea, and T. M. Truskett, J. Chem. Phys. **145**, 054901 (2016).

[34] D. Ormrod Morley and M. Wilson, J. Phys.: Condens. Matter **30**, 50LT02 (2018).

[35] D. Ormrod Morley and M. Wilson, Mol. Phys. **117**, 3148 (2019).

[36] M. E. Fisher, Phys. Rev. **124**, 1664 (1961).

[37] P. W. Kasteleyn, Physica **27**, 1209 (1961).

[38] V. A. Gorbunov, S. S. Akimenko, and A. V. Myshlyavtsev, Phys. Chem. Chem. Phys. **19**, 17111 (2017).

[39] D. Nieckarz, W. Rzysko, and P. Szabelski, Phys. Chem. Chem. Phys. **20**, 23363 (2018).

[40] C. Buzano, E. De Stefanis, A. Pelizzola, and M. Pretti, Phys. Rev. E **69**, 061502 (2004).

[41] N. Metropolis, A. W. Rosenbluth, M. N. Rosenbluth, A. H. Teller, and E. Teller, J. Chem. Phys. **21**, 1087 (1953).

[42] A. Kumar, M. Wilson, and M. F. Thorpe, J. Phys.: Condens. Matter **24**, 485003 (2012).

[43] G. T. Barkema and N. Mousseau, Phys. Rev. B **62**, 4985 (2000).

[44] A. Kumar, D. Sherrington, M. Wilson, and M. F. Thorpe, J. Phys.: Condens. Matter **26**, 395401 (2014).

[45] A. Gervois, J. P. Troadec, and J. Lemaitre, J. Phys. A **25**, 6169 (1992).

[46] M. P. Miklius and S. Hilgenfeldt, Phys. Rev. Lett. **108**, 015502 (2012).

[47] S. Le Roux and F. Rezai-Aria, J. Phys. D **46**, 295301 (2013).

[48] S. N. Chiu, Mater. Charact. **34**, 149 (1995).

[49] M. E. J. Newman, Phys. Rev. Lett. **89**, 208701 (2002).

[50] N. Rivier, D. Weaire, and R. Romer, J. Non. Cryst. Solids **105**, 287 (1988).

[51] See Supplemental Material at http://link.aps.org/supplemental/10.1103/PhysRevE.102.062308 for a discussion of system size effects in procrystalline lattices.

[52] P. J. Camp, Phys. Rev. E **68**, 061506 (2003).

[53] M. Griebel and J. Hamaekers, Comput. Mater. Sci. **39**, 502 (2007).

[54] A. Malashevich, S. Ismail-Beigi, and E. I. Altman, J. Phys. Chem. C **120**, 26770 (2016).

[55] D. A. Aboav, Metallography **13**, 43 (1980).

[56] B. N. Boots, Metallography **17**, 411 (1984).

[57] H. J. Hilhorst, J. Phys. A **39**, 7227 (2006).

[58] J. K. Mason, R. Ehrenborg, and E. A. Lazar, J. Phys. A **45**, 065001 (2012).

[59] A. Simonov, T. D. Baerdemaeker, H. L. B. Boström, M. L. R. Gómez, H. J. Gray, D. Chernyshov, A. Bosak, H.-B. Bürgi, and A. L. Goodwin, Nature (Lonson) **578**, 256 (2020).

[60] M. Florescu, S. Torquato, and P. J. Steinhardt, Proc. Natl. Acad. Sci. USA **106**, 20658 (2009).

[61] S. R. Sellers, W. Man, S. Sahba, and M. Florescu, Nat. Commun. **8**, 14439 (2017).